

Microw. Radiomet. Remote Sens. Earth's Surf. Atmosphere, pp. 433-443
P. Pampaloni and S. Paloscia (Eds)
© VSP 2000

Automatic self-calibration of ARM microwave radiometers

JAMES C. LILJEGREN

DOE Ames Laboratory, Ames, IA 50011, USA

Abstract—Microwave radiometers deployed in remote locations by the Atmospheric Radiation Measurement (ARM) Program must operate continuously and autonomously. In order to assure that their calibrations are maintained I have developed algorithms that permit these instruments to automatically self-calibrate when clear sky conditions are detected. First, basic calibration principles for these radiometers are reviewed. Algorithms that correct for misalignment of the elevation angle-scanning mirror and the finite width of the antenna beam pattern are described next. The automatic calibration scheme is then presented along with examples of its performance.

1. INTRODUCTION

The U. S. Department of Energy (DOE) Atmospheric Radiation Measurement (ARM) Program [1] has deployed dual-channel microwave radiometers in rural Oklahoma and Kansas, the north slope of Alaska, and on islands in the tropical Pacific Ocean. These radiometers are to provide continuous measurements of integrated water vapor (IWV) and integrated liquid water (ILW) amounts. Due to the remote nature of these locations, several weeks or months may elapse between maintenance visits by operations personnel. Even then, subtle problems that can adversely affect the instrument calibrations may go undetected. This necessitates expensive post-calibration and reprocessing efforts that substantially delay delivery of the data to the end users. In order to assure that the radiometer calibrations are correctly maintained, algorithms that permit them to be automatically and continuously updated have been developed and implemented.

In this paper the principles of radiometer calibration, as applied to these instruments, are first briefly reviewed. Algorithms that correct for misalignment of the elevation angle scanning mirror and for finite beam width effects are described next. Finally, the algorithms that permit the radiometer calibration to be automated are discussed and examples presented to demonstrate their performance.

2. CALIBRATION PRINCIPLES

The ARM microwave radiometers provide the equivalent blackbody brightness temperature, T_{sky} for each channel (refer to Table 1 for specifications) according to:

$$T_{\text{sky}} = T_{\text{ref}} + G (V_{\text{sky}} - V_{\text{ref}}) f_w. \quad (1)$$

V_{sky} is the signal recorded when the reflector is oriented toward the sky; the mirror is then pointed downward to view the internal blackbody reference target and V_{ref} is recorded. T_{ref} is the measured temperature of the reference target. The factor $f_w = 1/(1-\epsilon)$ accounts for the polycarbonate foam window covering the mirror; ϵ is the window emissivity. G is the calibrated gain calculated as

$$G = T_{\text{nd}} / (V_{\text{ref+nd}} - V_{\text{ref}}). \quad (2)$$

$V_{\text{ref+nd}}$ is the signal when viewing the reference target with the noise diode energized. T_{nd} is the noise injection temperature that must be determined by prior calibration.

Because the noise diode is maintained at a constant temperature (± 0.25 K), its output is constant. However, because the antenna and feedhorn are not thermally stabilized, the value of T_{nd} can exhibit a slight dependence on the temperature inside the radiometer enclosure, which is equal to the temperature of the reference target T_{ref} . This temperature dependence is determined in the calibration procedure.

Table 1. Specifications of the Radiometrics WVR-1100 microwave radiometers used by ARM.

	Vapor-sensing channel	Liquid-sensing channel
Frequency	23.8 GHz	31.4 GHz
Bandwidth	0.4 GHz	0.4 GHz
Beamwidth (FWHP)	5.9 degrees	4.5 degrees
Window emissivity	0.00164	0.00217

2.1 Tip Curves

The noise injection temperature T_{nd} is calculated by combining Eq. 1 and Eq. 2,

$$T_{\text{nd}} = \frac{T_{\text{sky}} - T_{\text{ref}}}{V_{\text{sky}} - V_{\text{ref}}} (V_{\text{ref+nd}} - V_{\text{ref}}) f_w^{-1}. \quad (3)$$

An independent measurement of T_{sky} is needed in order to determine T_{nd} . For horizontally homogeneous, clear sky conditions the optical thickness or opacity $\tau(\theta)$ at an elevation angle θ is proportional to the zenith opacity τ_{zen}

$$\tau(\theta) = \tau_{\text{zen}} m(\theta); \quad (4)$$

m is a mapping function that describes the ratio of the path length through the atmosphere at θ to the path length at zenith. This ratio is also known as the airmass. (For a plane-parallel atmosphere, $m = 1/\sin \theta$.) The relationship in Eq. 4 is exploited to provide an

independent measurement of T_{sky} . An old or estimated value of T_{nd} is used to obtain values of T_{sky} for 10 angles corresponding to $m = 1, 1.5, 2, 2.5,$ and 3 . The opacities are calculated according to

$$\tau = \ln \left(\frac{T_{mr} - T_{bg}}{T_{mr} - T_{sky}} \right). \quad (5a)$$

T_{mr} is the atmospheric mean radiating temperature, which may be estimated from climatology ($\sim 2\%$ accuracy) or from surface temperature and relative humidity ($\sim 1\%$ accuracy) [2]. T_{bg} is the cosmic background radiating temperature (2.73 K).

A linear regression of τ on m (i.e., a tip curve as illustrated in Fig. 1) is then computed. The slope of the regression is an estimate of τ_{zen} . If the correlation coefficient of the regression $R \geq R_{min}$ (I use $R_{min} = 0.998$), indicating that Eq. 4 is obeyed, then the tip curve is said to be "valid" and this estimate of τ_{zen} is used to estimate T_{sky} :

$$T_{sky} = T_{bg} e^{-\tau} + T_{mr} (1 - e^{-\tau}). \quad (5b)$$

This value is substituted into Eq. 3 to obtain an improved estimate of T_{nd} . This process is repeated with the new estimate of T_{nd} until the intercept of the regression converges to zero, as required by Eq. 4. (Normally, only one iteration is needed.)

3. CALIBRATION ERRORS AND CORRECTIONS

An error in the calibration δT_{nd} causes an error in the measured brightness temperature δT_{sky} given by

$$\delta T_{sky} = \delta T_{nd} (T_{ref} - T_{sky}) / T_{nd}. \quad (6)$$

Because $|T_{ref} - T_{sky}| / T_{nd} \approx 1$, $|\delta T_{sky}| \approx \delta T_{nd}$. The ARM microwave radiometers can scan 10 elevation angles and acquire a complete tip curve in about 50 seconds. This allows about 1500 valid tip curves per day to be acquired if the sky remains clear such that $R \geq 0.998$. Although statistical errors due to an insufficient number of tip curves can be kept very small, such errors can arise from offsets in the elevation angle of the mirror which reduce R . Additionally, systematic (bias) errors can arise due to the finite width of the antenna beam pattern. Both of these issues are addressed in the automatic calibration scheme.

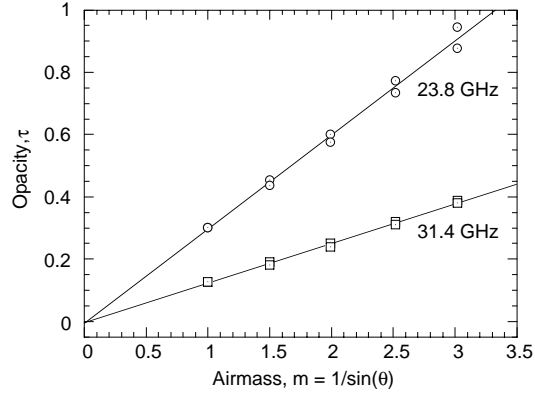


Figure 1. Typical tip curves. The divergence of the data points, especially at 23.8 GHz, is due to an offset error in the elevation angle, and is now corrected automatically.

3.1 Mirror Alignment

Due to continuous use, the mirrors on some of the ARM radiometers have slipped as much as 1° on their stepper motor shafts. The resulting offset in elevation angle causes the brightness temperatures and opacities to be measured at different airmasses than specified. This problem is evident in Fig. 1. Although the regression of τ on m gives the same value of τ_{zen} as for the case of zero offset, the scatter about the regression line increases substantially. Consequently, many or most tip curves do not pass the screening criterion ($R \geq 0.998$) and the resulting calibration is based on a sharply reduced number of samples. If the screening criterion were relaxed, say to 0.995, then some cloud-contaminated tip curves could be accepted as valid which could bias the calibration.

To correct for this, the angular offset is calculated for angles $\theta \geq 150^\circ$ and $\theta \leq 30^\circ$:

$$\begin{aligned} \Delta\theta &= \sin^{-1}(\tau_{zen} / \tau) - \theta, \quad \theta \leq 30^\circ; \\ \Delta\theta &= [180 - \sin^{-1}(\tau_{zen} / \tau)] - \theta, \quad \theta \geq 150^\circ. \end{aligned} \quad (7)$$

The median offset is then computed for each tip curve of the liquid-sensitive (31.4 GHz) channel and stored. The liquid water-sensing channel is used for this purpose rather than the vapor-sensing channel (or both) to minimize the possibility that a persistent horizontal gradient in water vapor could be mistaken for an elevation angle offset. Each hour the

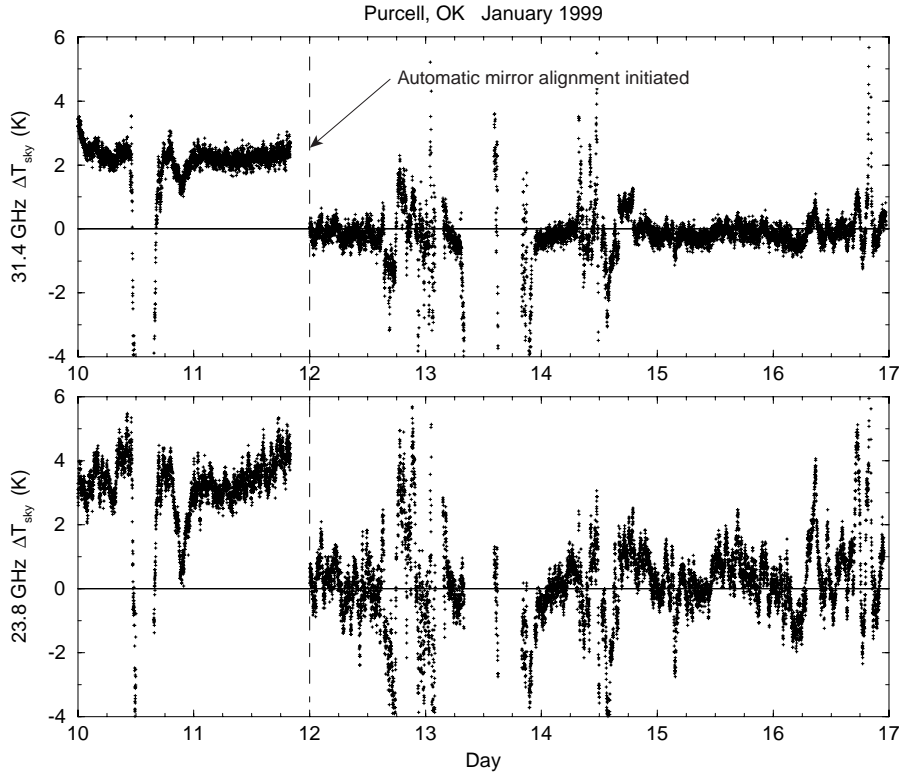


Figure 2. Brightness temperature differences for $m = 3$ (T_{sky} at $\theta = 19.5^\circ$ minus T_{sky} at 160.5°).

median offset angle for the most recent clear-sky tip curves (up to 1000) is computed and converted to an integer number of motor steps (0.45° per step). If the offset is a non-zero number of steps, the elevation mirror position is adjusted to account for it.

As shown in Fig. 2 (for $m = 3$), after this algorithm was installed, the bias in the clear-sky differences T_{sky} at $\theta = 19.5^\circ$ minus T_{sky} at 160.5° was reduced to zero. Similarly, the correlation coefficient of the tip curve regressions increased to $R \geq 0.999$.

3.2 Beam Correction

The antenna temperature $T_{\text{ant}}(\theta_o)$ measured by a radiometer along a line-of-sight path at an elevation angle θ_o represents a convolution of $T_{\text{sky}}(\theta)$ with the antenna power pattern P ,

$$T_{\text{ant}}(\theta_o) = \int T_{\text{sky}}(\theta) P(\theta - \theta_o) d\theta. \quad (8)$$

The power pattern is assumed to be radially symmetric. Azimuthal variations in T_{sky} are assumed negligible in comparison with elevational variations.

Because T_{sky} varies non-linearly with θ , T_{ant} is always greater than the value of T_{sky} at the beam center. The effective elevation angle, given by $T_{\text{ant}}(\theta) = T_{\text{sky}}(\theta_{\text{eff}})$, is always closer to the horizon than the actual angle; the effective airmass $m_{\text{eff}} = \tau_{\text{eff}} / \tau_{\text{zen}}$ is always greater than the actual value. To correct for this effect, Eq. 8 must be evaluated for a given zenith opacity τ_{zen} to yield T_{ant} , which is substituted into Eq. 5a to give τ_{eff} and finally m_{eff} is determined. Tip curve regressions can then be carried out using m_{eff} .

In order to evaluate Eq. 8, the radiometer antenna is modeled as a circular aperture with a parabolic amplitude taper because the primary beam-forming element is the Gaussian optics lens [3]:

$$g(\theta) = 8 J_2(\beta a \sin \theta) / (\beta a \sin \theta)^2; \quad \beta = 2\pi/\lambda. \quad (9)$$

J_2 is the second order Bessel function of the first kind, a is the radius of the aperture (7.6 cm) and λ is the wavelength. The resulting power pattern $P(\theta) = [g(\theta)]^2$ for $\lambda = 1.2605$ cm (23.8 GHz), plotted in Fig. 3a, has a half-power beam width of 6° which is very close to the value of $5.7\text{-}5.9^\circ$ supplied by Radiometrics; the first sidelobe is -25 db at 10° from

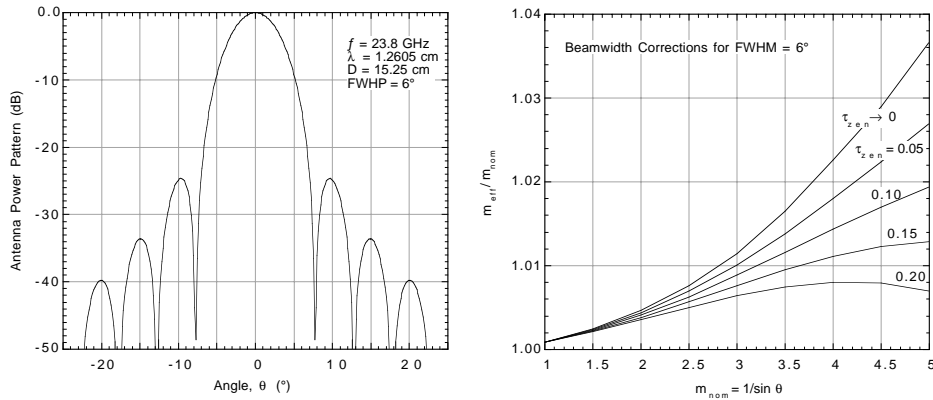


Figure 3. (a) The radiometer beam pattern. (b) Beamwidth corrections for the 23.8 GHz channel.

the main beam axis, also in agreement with the Radiometrics data. At 31.4 GHz the calculated half-power beam width is 4.5° , in close agreement with the Radiometrics measurements ($4.5\text{-}4.7^\circ$).

The mirror intercepts the beam at angles $\leq 12.5^\circ$ (the second null in the pattern at 23.8 GHz). An absorbing collar intercepts sidelobes beyond 21.5° . Between 12.5° and 21.5° the sidelobes "spill over" the mirror; however, the antenna gain is -33 dB or less and the contribution is negligible. Even if it were not negligible, it would not vary during the time that tip curve measurements are acquired (50 seconds). Consequently, because any "spill over" contribution is common to the blackbody and sky measurements it is eliminated by the $V_{sky} - V_{ref}$ difference in Eq. 1. (Radiometer designs that do not permit rapid angular scanning and do not include a blackbody target in their observing cycle are susceptible to "spill over" errors.)

The variation of T_{sky} with θ was modeled using Eq. 4 and Eq. 5b. Because the convolution in Eq. 8 is over all angles, the plane-parallel mapping function ($m = 1/\sin \theta$) was replaced by the Niell wet mapping function [4], which describes a spherical atmosphere with a scale height corresponding to water vapor. This is necessary because $1/\sin \theta \rightarrow \infty$ as $\theta \rightarrow 0$, so using the plane-parallel assumption would result in over-correction. The resulting corrections are presented in Fig. 3b in terms of the ratio m_{eff} / m_{nom} , where $m_{nom} = 1/\sin \theta$.

4. AUTOMATIC CALIBRATION

The first step in the automatic calibration procedure, summarized in Fig. 4, is to assess whether the sky is sufficiently clear. To do this, a 30-minute running mean and standard deviation of integrated liquid water are calculated. When the standard deviation falls below 0.008 mm ($2 \times$ RMS noise level), the radiometer begins acquiring

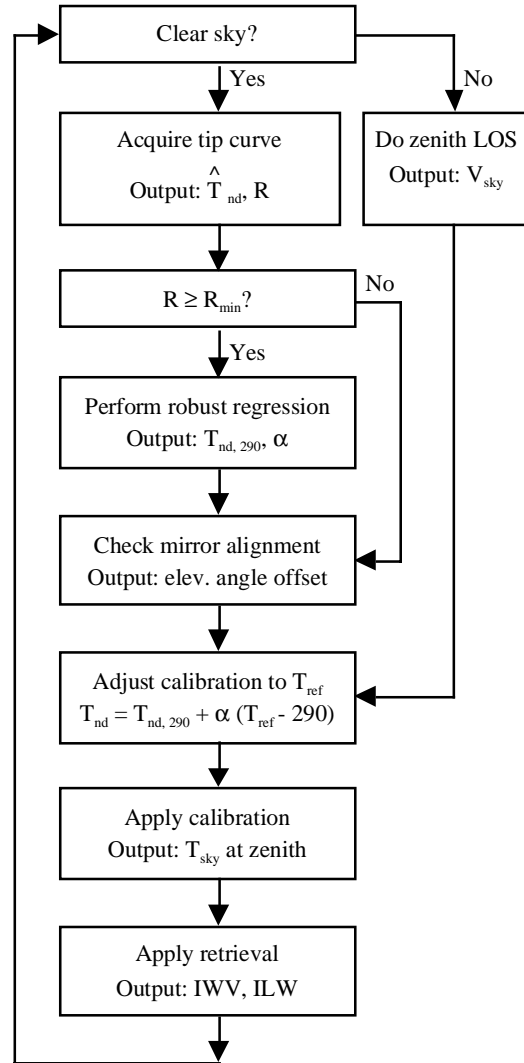


Figure 4. Flowchart of automatic calibration.

tip curves. If a tip curve is valid ($R \geq R_{\min}$), the instantaneous value of T_{nd} is stored in a circular array containing the most recent (up to 3000) values of T_{nd} and T_{ref} . Once a minimum number of valid tip curves have been acquired, a robust linear regression (least absolute deviation) of T_{nd} on T_{ref} is then carried out each time a new value of T_{nd} is acquired. This yields a continuously updated estimate of $T_{\text{nd}, 290}$ (the value of T_{nd} at $T_{\text{ref}} = 290$ K) and a temperature coefficient α for each channel. These are used to continuously predict T_{nd} from T_{ref} :

$$T_{\text{nd}} = T_{\text{nd}, 290} + \alpha (T_{\text{ref}} - 290). \quad (10)$$

The robust regression is employed to prevent outliers from affecting the calibration. Outliers can result when the horizontal water vapor distribution is not homogeneous. When the sky is not clear the radiometer measures T_{sky} along a zenith line-of-sight (LOS) only using the most recent values of $T_{\text{nd}, 290}$ and α from the automatic calibration algorithm to adjust T_{nd} for the given T_{ref} based on Eq. 10.

Time series of T_{nd} are presented in Fig. 5 for January 10-30, 1999. A running 2-hour median of the instantaneous values is plotted to indicate the central tendency. It appears

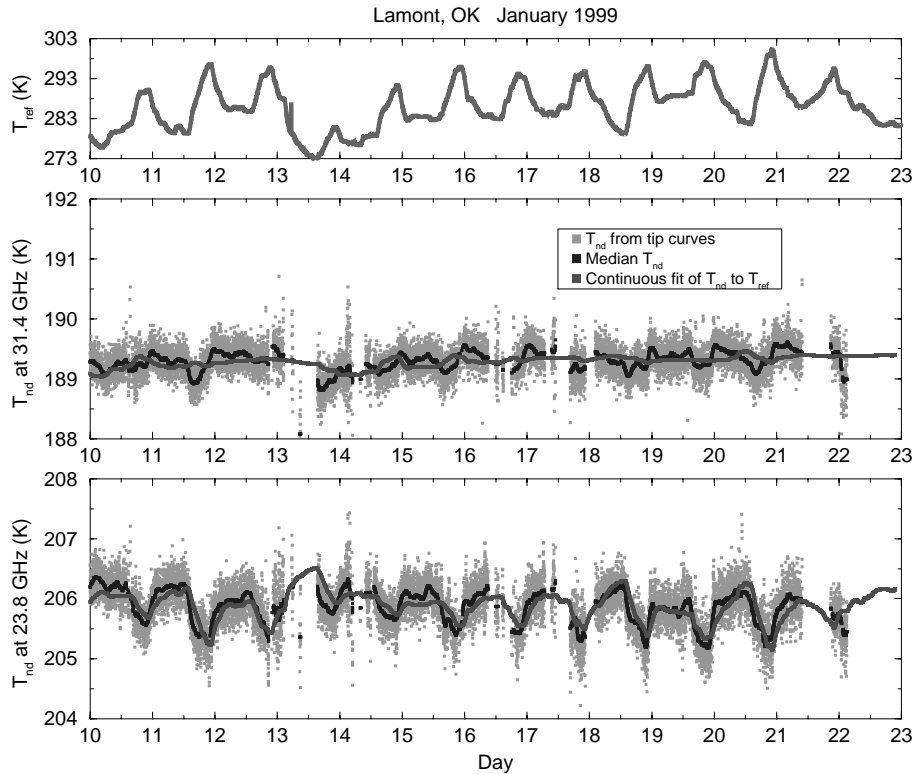


Figure 5. Top panel: time series of reference temperature T_{ref} . Middle and lower panels: time series of noise injection temperature T_{nd} for the 31.4 and 23.8 GHz channels from individual tip curves (light grey), a 2-hour running median (black), and predicted from the continuous fit to T_{ref} (dark grey). Gaps indicate cloudy sky periods when no tip curves were acquired.

Automatic self-calibration of ARM microwave radiometers

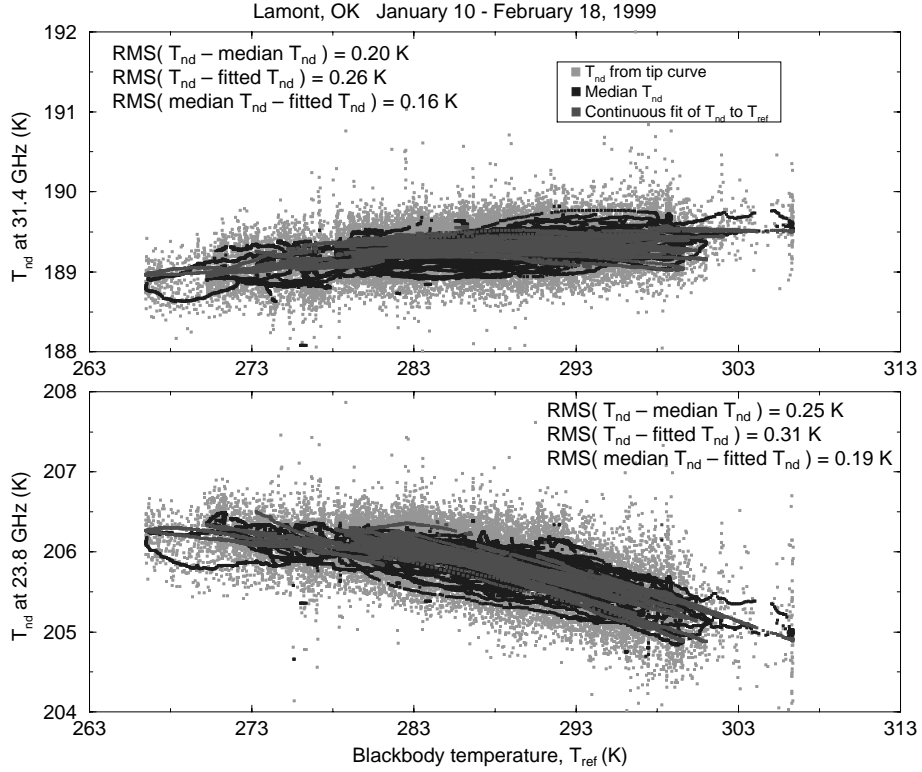


Figure 6. The dependence of T_{nd} on T_{ref} at 31.4 GHz (top panel) and 23.8 GHz (lower panel). For this instrument, the 31.4 GHz channel is nearly independent of T_{ref} .

that the value of T_{nd} predicted from T_{ref} tracks the median better at 23.8 GHz than at 31.4 GHz. However, the variations in T_{nd} at 31.4 GHz are considerably smaller than at 23.8 GHz. It is also apparent from the plots of T_{nd} vs. T_{ref} presented in Fig. 6 that the values of T_{nd} at 23.8 GHz exhibit a much greater correlation with T_{ref} . In any case, the RMS difference between the predicted values of T_{nd} and the running median is less than 0.2 K for both channels. Thus $\delta T_{nd} \approx 0.2$ K. Referring to Eq. 6, this gives $\delta T_{sky} = 0.2-0.3$ K.

5. CONCLUSIONS

A continuous, automatic self-calibration procedure has been developed and implemented for ARM microwave radiometers. Algorithms have been developed to automatically align the elevation angle-scanning mirror and correct for finite beam width effects. This procedure maintains the radiometer calibration to 0.2-0.3 K RMS.

Acknowledgement. This work was supported by the Environmental Sciences Division of the U.S. Department of Energy under the auspices of the Atmospheric Radiation Measurement (ARM) Program. The Ames Laboratory is operated for the U.S. Department of Energy by Iowa State University.

James C. Liljegren

REFERENCES

1. G. M. Stokes and S. E. Schwartz, "The atmospheric radiation measurement (ARM) program: programmatic background and design of the cloud and radiation test bed," *Bull. Amer. Met. Soc.*, **75**, 1201-1221 (1994)
2. J. C. Liljegren, "Improved retrieval of cloud liquid water path," Preprints of the 10th Symposium on Meteorological Observations and Instruments, January 11-16, 1998, Phoenix, AZ.
3. W. L. Stutzman, and G. A. Thiele, *Antenna Theory and Design*, 2nd Ed., John Wiley and Sons, New York. (1998)
4. A. E. Niell, A. E., "Global mapping functions for the atmosphere delay at radio wavelengths," *J. Geophys. Res.*, **101**, 3227-3246 (1996)